META-STABILITY IN ATMOSPHERIC JETS

Nayef Shkeir and Tobias Grafke

Mathematics for Real-World Systems CDT, Zeeman Building, University of Warwick

(Dated: 1 October 2020)

Turbulence in atmospheres, oceans and plasma flows leads to coherent large-scale jets that persist for long-times. These jets may be steady or transition between several meta-stable jet configurations. We study the dynamics of these atmospheric jets on large rotating Jovian planets where we can apply the stochastically forced two-dimensional barotropic equation in the β-plane. Direct numerical simulation of the quasi-linear approximation of this system is presented with verification of large time-scale separation between the slow zonal evolution and fast vorticity fluctuations. We exploit this time-scale separation property and apply the classical tool of stochastic averaging to obtain a closed limiting equation for the zonal evolution while averaging out the non-zonal fluctuations in the turbulent inertial regime $\nu \ll \alpha \ll 1$. This tool is used to numerically compute multiple meta-stable jet configurations for various parameter values and a bifurcation analysis on the number of stable jets is carried out by varying the non-dimensional parameter Coriolis β. We find that the novel tool developed in this report is extremely useful to efficiently compute the dynamics of systems that exhibit large time-scale separation.

I. INTRODUCTION

Large-scale coherent structures such as jets are seen to emerge in turbulent background velocity fields. For planets with a circulating atmosphere, jets are commonly the largest and most persistent features seen in the atmosphere. Such structures have been extensively observed such as the time-dependent banded winds recorded by the Voyager missions in 1979 on gaseous Jovian planets[1] (Jupiter, Saturn, Uranus and Neptune) and the slow, large-scale torsional oscillations about the Sun's equator[2]. For the Earth's atmosphere, the jets show much more stochasticity in structure such as the meandering jet stream and usually have a smaller number of jets compared to Jovian planets.

Jupiter's jets are very stable as very little differences were seen in the atmosphere and jet structure between the Voyager (1979) and Cassini probes (2000). It is, however, believed that Jupiter did indeed lose a jet in the 1940s where white ovals formed as a substitute and Jupiter's atmosphere dramatically changed[3]. The stability of jet configurations is therefore of great importance to the scientific community of not only Jupiter but also other planets in our universe including Earth.

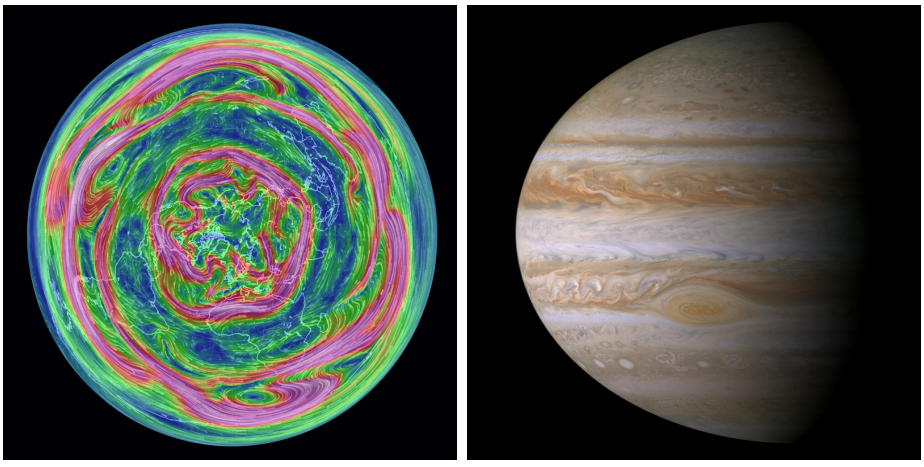

FIG. 1: Left: Image of Earth's north pole showing jet streams. Image taken from weather conditions visualiser by Cameron Beccario. Right: A profile of Jupiter's atmosphere showing clear banded zonal jets. Image taken by NASA's Cassini probe.

In atmospheric flows, geostrophic turbulence exists as a result of the geostrophic balance between the Coriolis force and the pressure gradient. More generally, turbulence in planetary atmospheres is a result of kinetic energy from planetary rotation, the deep atmosphere and heat sources which drive circulations in a planets atmosphere and/or ocean. Thermal energy is converted (through complex processes) to kinetic energy from heat sources such as a planet's primary sun and the internal heat of a planet. This turbulence leads to the formation of coherent, banded and long-lasting zonal jets (flowing east to west). There are currently two agreed-upon mechanisms for the formation/maintenance of jets on giant planets; "shallow" forcing and "deep" forcing[4]. In "shallow" forcing, the jets are driven by processes such as moist convection in the outermost layers of the atmosphere. Whereas, in "deep" forcing, convection in the planet's interior and the rotation of the planet induces Rossby waves which are amplified by an inverse energy cascade. Rhines first proposed the inverse energy cascade where energy from the small-scale eddies (swirling fluid) accumulates in larger scales which causes Rossby waves to be more significant over time[5]. Rossby waves dominate the flow when they travel faster than the root-mean-square of the turbulent velocity field which leads to elongation of the eddies and therefore, the formation of jets. Numerical studies have shown that jets also emerge from turbulent flow without an energy cascade[6], therefore, there must be other mechanisms which lead/aid in jet formation.

Many theoretical works have used the assumption of a barotropic system. This involves treating the atmosphere as a homogeneous fluid which is an approximation as planetary atmospheres are stratified (baroclinic). In a barotropic model, jets form unconditionally whereas, in a baroclinic model, a limit exists on Rossby wave magnitude which makes jet formation conditional on this limit. Williams et al.[7] suggests that Rossby wave velocity magnitude must be six times larger than the velocity of the turbulent velocity field for jet emergence, much larger than in barotropic flow. Throughout this report, we use the barotropic assumption for simplicity.

The formation of zonal jets has been studied extensively in experimental as well as theoretical settings. Sommeria et al.[8] identified similar (eastward) jets as seen in planetary currents using a radially rotating sloping annulus with varying mechanical forcing. Nitto et al.[9] found zonal jets in a square rotating tank with electromagnetic forcing of a shallow layer of fluid which replicates the dynamics of the atmosphere in the polar regions. Even in these small-scale experiments, zonal jets are seen and persist for long-times in the presence of eddy mixing. However, the Reynolds number is very high in atmospheric flows which is currently not reproducible in a laboratory.

Most theoretical research in geophysical flows has been carried out on 2-D turbulence as opposed to 3-D turbulence. In 2-D turbulence, an inverse energy cascade exists whereas, in 3-D turbulence, the energy cascade is forward (large-scales to small-scales) as many more instabilities exist. Nevertheless, turbulence in 3-D atmospheric flows has the same dynamical invariants (energy and enstrophy for example) as the 2-D system which as a result means that phenomena such as large-scale structure formation can be modelled by a 2-D system.

Turbulence must be spatially organised for the maintenance of zonal jets and there are no known external mechanisms which lead to this maintenance. Therefore, the jets themselves must organise the turbulent eddy field which in turn organises the jets (positive-feedback). This mechanism is called shear-straining as the jets induce a phase-tilt in isotropic eddies. However, more theoretical and experimental work is needed to confirm this positive-feedback as the evidence is scarce. Jets can also spontaneously emerge without the organisation of Rossby waves as a result of a potential-vorticity (PV) staircase where Rossby waves break at regions of weak PV, which as a result weakens the PV gradient at these regions. This forms a staircase pattern and it has been shown that when a PV staircase exists, jets do also[10].

In simple terms, the jet velocity profile can be said to be determined by the continuous balance between the forcing (non-zonal turbulent fluctuations) and the dissipation (viscosity and friction). These zonal jets travel at greater velocities relative to the planetary surface and are critical to the study of planetary climate as they are involved in the transfer of angular momentum, heat and particulates in an atmosphere[1]. Very similar jet structures can also be found in plasma flows in magnetic plasma confinement devices where the efficiency of plasma confinement can be affected by jet formation[11].

An alternative explanation of jet formation has been given by Onsager[12] using statistical equilibrium theory which states that turbulence will tend to organise in configurations which maximise entropy and in 2-D turbulence, zonal jets and large eddy configurations have the largest entropy[13]. Using statistical equilibrium theory is very useful in this setting as there are a large number of degrees of freedom due to non-linear eddy interactions. This method built upon by Robert et al.[14] involves solving the unforced 2D Euler equations for maximal entropy which results in either jets[15] or large vortex structures[16]. However, as this method involves an unforced system, the application

to atmospheres is tentative as planetary atmospheres can be highly forced and not in equilibrium.

A natural approach to study the dynamics of turbulent flow is to obtain the Probability Density Function (PDF) as a state variable which would provide all the statistics of turbulence. However, the PDF is very difficult to obtain or to even approximate by sampling state trajectories. Farrell and Ioannou[17] propose to use statistical variables for the dynamics as opposed to state variables when studying complex turbulent systems. An argument is made that to gain insight into time-dependent turbulent equilibria, adopting statistical variables is imperative as statistics obtained from sampling realisations would not be representative of the statistical state at any time. This perspective, called Statistical State Dynamics (SSD), was first applied by Hopf[18] where he studied turbulence by formally expanding in cumulants. Bouchet et al.[19] recently adopted SSD to study the kinetic theory of the 2D stochastic barotropic equation using the Fokker-Planck equation to describe the velocity evolution in jets in the limit of weak forces and dissipation. A popular implementation of SSD is Stochastic Structural Stability Theory (S3T) which is a second-order cumulant expansion (CE2)[20] with stochastic parameterisation and also the deterministic part of the Fokker-Planck equation at leading order[21]. S3T dynamics uses the idealisation of an infinite ensemble of perturbations of the fast variable such as vorticity acting on the mean slow variable such as velocity and has been extensively used in the study of barotropic turbulence[6,22,23].

The method proposed in this report (stochastic averaging) is similar to S3T, however, we do not evolve the covariance of perturbations but instead consider the steady-state of the perturbations acting on the mean zonal flow to compute fixed points in the system. This is much more efficient as we are finding fixed points in a deterministic system instead of a stochastic one. We have achieved this by exploiting the existence of a time-scale separation between the variables in a system by decoupling them explicitly. Related methods have been proposed before such as the heterogeneous multiscale method (HMM)[24] which has been applied in molecular dynamics and biological systems[25], however, stochastic averaging has a much more rigorous basis. This is the first example of work that has successfully implemented stochastic averaging to efficiently compute meta-stable jet configurations for the quasi-linear (QL) barotropic system.

The structure of the report is as follows; In section II, we introduce the non-linear 2D stochastically forced barotropic equation and non-dimensionalise the system to three dimensionless parameters. We also define the structure of forcing used throughout this report. In section III, we decompose the variables in the system to zonal and non-zonal parts to obtain the QL approximation and we then define our numerical method and integrate the system for various parameters. In section IV, we introduce a method to compute meta-stable jet configurations in the limit of large time-scale separation between the fast and slow variables. We then use this method to compute meta-stable states and investigate the parameter space much faster than integrating the QL system which would not be possible without stochastic averaging. We finally conclude our report and present future work in section V.

II. 2D QUASI-GEOSTROPHIC DYNAMICS IN THE β-PLANE

At a simplified level, the atmosphere can be viewed as a 2D homogeneous (barotropic) fluid on a rotating sphere. In this setting, the Coriolis parameter, f, defined as $f = 2\Omega \sin\theta$, depends on latitude where Ω is the angular velocity of planetary rotation and θ is the latitude. Therefore, Taylor expanding around a latitude θ_0 and retaining only the linear term gives $f = f_0 + \beta_d y$ where $\beta_d = (1/a)df/d\theta|_{\theta_0}$ where a is the planetary radius, this is the beta-plane approximation. This approximation is very useful as it does not contribute non-linear terms to the system and includes Coriolis variation with latitude. We therefore consider the (non-linear) 2D stochastically forced barotropic equation in the β-plane on a periodic domain $\mathcal{D} = [0, 2\pi l_x L) \times [0, 2\pi L)$ (in order to avoid boundary effects) where $1/l_x$ is the aspect ratio:

$$\partial_t \omega + \boldsymbol{v} \cdot \nabla \omega + \beta_d v = -\lambda\omega - \nu(-\Delta)^p \omega + \sqrt{\gamma}\eta\,, \tag{1}$$

where $\boldsymbol{v} = (u, v) = \boldsymbol{e}_z \times \nabla\psi$ is the velocity field for a stream function $\psi(x, y)$, $\omega = \Delta\psi$ is the vorticity and $\Delta = \partial_{xx} + \partial_{yy}$ is the Laplacian operator. In the equation above, $\boldsymbol{r} = (x, y)$ are space vectors where y is the meridional coordinate and x is the zonal coordinate (where x and y are Cartesian coordinates). The beta effect is present with β_d, λ is the Ekmann friction coefficient which dissipates flow, γ is the energy input rate and ν is the hyper-viscosity (or viscosity when $p = 1$) coefficient. As the fields are periodic, $f(x + 2\pi l_x L, y) = f(x, y)$ and $f(x, y + 2\pi L) = f(x, y)$. Depending on the value of β_d, this system transfers energy into the zonal shear modes

TABLE I: Typical values of relevant physical parameters. L is the forcing length scale, $1/\lambda$ is the dissipation time scale and β_d is the dimensional beta-effect value. Values obtained from Bakas and Ioannou[22].

	L (km)	$1/\lambda$ (days)	β_d $(10^{-11}m^{-1}s^{-1})$
Earth's Atmosphere	1000	10	1.6
Earth's Ocean	20	100	1.6
Jovian Atmosphere	1000	1500	0.35

and evolves the turbulence. A forcing term, η, is introduced as random stirring to sustain turbulence and account for energy cascades and small-scale convection. The forcing is chosen to be white in time, spatially homogeneous and isotropic, concisely represented as $\mathbb{E}\left[\eta(\boldsymbol{r}_1,t_1)\eta(\boldsymbol{r}_2,t_2)\right]=\delta(t_2-t_1)\chi(|\boldsymbol{r}_2-\boldsymbol{r}_1|)$ with the expectation taken over noise realisations where χ is the two-point, one time correlation function which is positive-definite. The property of zonal translational invariance is physically correct and important for the computations carried out in this report. In the absence of dissipation and forcing, the energy,

$$E=\frac{1}{2}\int_{\mathcal{D}}\boldsymbol{v}^2 d\boldsymbol{r}, \tag{2}$$

is conserved and the system models perfect barotropic flow.

A. Non-dimensionalisation

We non-dimensionalise the system as carried out by Bouchet[19] for consistency. The noise is a white in time Gaussian process for which the average can be computed a-priori and so we normalise the noise such that $-2\pi^2 l_x L^2(\Delta^{-1}\chi)(\boldsymbol{0})=1$. With this normalisation, the average input energy is γ and multiplying χ by a positive constant would renormalise γ. If we neglect hyper-viscosity, the energy balance for Eq.(1) in a statistically stationary regime is $E_{st}:=\mathbb{E}[E]\approx\gamma/2\lambda$ which is the approximate average energy.

We rescale the system to non-dimensional parameters such that the new domain size is $\mathcal{D}=[0,2\pi l_x)\times[0,2\pi)$ and the average energy is unity. We do this by defining non-dimensional time as $t'=t/\tau$ where $\tau=L^2\sqrt{2\lambda/\gamma}$ and a non-dimensional spacial variable $\boldsymbol{r}'=\boldsymbol{r}/L$. We rescale the physical variables as $\omega'=\tau\omega$, $v'=\tau v/L$, $u'=\tau u$, $\beta'=L\tau\beta_b$ and $\nu'=\nu\tau L^{-2p}$. A non-dimensional parameter is defined as $\alpha=\lambda\tau$ which is the ratio of the inertial and dissipative time-scales. We also rescale the stochastic Gaussian field as $\mathbb{E}\left[\eta'(\boldsymbol{r}_1',t_1')\eta'(\boldsymbol{r}_2',t_2')\right]=\delta(t_2'-t_1')\chi'(|\boldsymbol{r}_2'-\boldsymbol{r}_1'|)$ with $\chi'(\boldsymbol{r}')=L^4\chi(\boldsymbol{r})$. Inputting the above into Eq.(1) gives

$$\partial_t\omega+\boldsymbol{v}\cdot\nabla\omega+\beta v=-\alpha\omega-\nu(-\Delta)^p\omega+\sqrt{2\alpha}\eta\,, \tag{3}$$

where we have dropped the primes to simplify notation. This has reduced the original system Eq.(1) to only three dimensionless parameters α, β and ν. α can be thought of as an inverse Reynolds number based on the large scale dissipation of energy and ν mainly acts at small scales and is the inverse Reynolds number based on hyper-viscosity. The forcing prefactor is a result of rescaling the time and spatial forcing correlation as $\sqrt{\gamma}\tau^2(\tau^{-1/2}L^{-2})=\sqrt{2\alpha}$. Every variable that is considered in the report from this section onwards is non-dimensional. The energy balance for Eq.(3) is

$$\frac{dE_{st}}{dt}=2\alpha(1-E_{st})+\nu\mathbb{E}[\int_{\mathcal{D}}\psi(-\Delta)^p\omega d\boldsymbol{r}]. \tag{4}$$

In the case of $\beta=0$, Eq.(3) reduces to the 2D Navier-Stokes equations.

B. Stochastic forcing structure

The forcing covariance, χ , is spatially homogeneous (translationary invariant) in all directions which means that

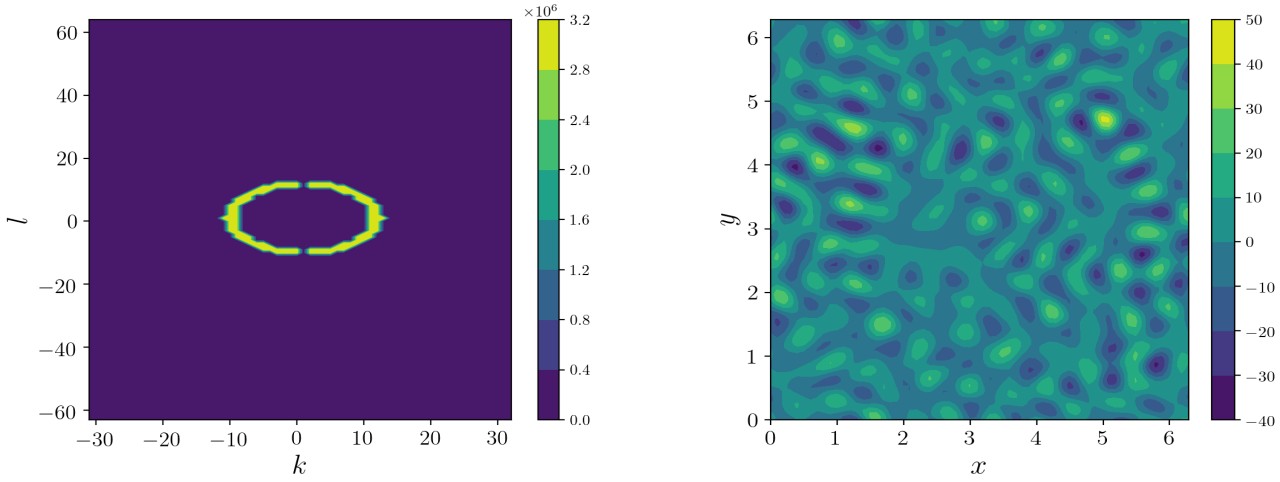

FIG. 2: Left: Non-dimensionalised $\hat{\chi}(k,l)$ on a 64×128 grid with $k_* = 11$ and $\delta k = 1$. Right: A realisation of the annulus forcing on the vorticity field. It can be seen that this type of forcing excites small-scale structures in the flow field.

$$\chi(\boldsymbol{r} + a) = \chi(\boldsymbol{r}), \tag{5}$$

where $a \in \mathbb{R}^2$. The covariance can then be written in terms of Euclidean distance instead of absolute coordinates and can therefore be written as the Fourier sum

$$\chi(x - x', y - y') = \sum_{k,l} \hat{\chi}(k,l) e^{ik(x-x') + il(y-y')}, \tag{6}$$

where $x - x'$ and $y - y'$ correspond to wavenumbers k and l and take integer values. We select a forcing which acts on a narrow annulus in wavenumber space such that

$$\hat{\chi}(k,l) = \frac{k_*}{\delta k} \begin{cases} 1, & \text{for } |\sqrt{k^2 + l^2} - k_*| \leq \delta k \\ 0, & \text{for } |\sqrt{k^2 + l^2} - k_*| > \delta k \end{cases}, \tag{7}$$

where k_* is the annulus radius and δk is the annulus width. We also choose not to force the zonal average, $\hat{\chi}(k = 0, l) = 0$. For a finite doubly periodic domain, the forcing is nearly isotropic and approaches exact isotropy as the domain size is increased. This forcing structure is common in 2D turbulence studies with inverse energy cascades and was first applied by Lilly[26] to study inverse cascades. Studies into β-plane turbulence have also used this forcing extensively[6,23]. For isotropic forcing, variation in the PV gradient causes eddy refraction and up-gradient momentum fluxes which causes instabilities and enhances the mean velocity flow[22].

Other forcing structures have been studied in relation to atmospheric turbulence such as considering a wider annular region around a central wavenumber and non-isotropic forcing which independently excites a set of zonal wavenumbers. Non-isotropic forcing was first applied by Williams at al.[27] to the study of baroclinic instabilities and has since been applied in S3T dynamics[21,23]. We assume that the forcing is independent of the velocity and vorticity fields. This assumption holds for Jovian atmospheres as the forcing is a result of thermal convection whereas this assumption would not hold for modelling Earth's jets for example as both the velocity and vorticity fields influence the forcing[22].

III. QUASI-LINEAR DYNAMICS

In this section we define the quasi-linear approximation of Eq.(3). We are mainly interested in the setting of $\alpha \ll 1$ as when this is the case, the large scale dissipation is very slow and is balanced by the Reynolds stress as a result of the turbulent fluctuations. When the velocity field approaches a jet configuration, $\boldsymbol{v} \approx U(y)\boldsymbol{e}_x$, this configuration evolves very slowly under the dissipation and stochastic forcing. We consider translational invariance along the zonal direction (x) in a statistical sense.

A. Decomposition into zonal and non-zonal components

Bouchet et al.[19] states that α describes a time-scale separation between the fast non-zonal fluctuations and the slow zonal fluctuations. The noise strength is of order $\sqrt{\alpha}$ therefore, it is natural to assume that the fluctuations are of order $\sqrt{\alpha}$ as the fluctuations are transferred to the large structures which are on a time-scale order of one. We, therefore split the velocity and vorticity in Eq.(3) into zonal and non-zonal components with a time-scale separation of $\sqrt{\alpha}$ between the zonal mean and the fast fluctuations. We define the mean $(\overline{\cdot})$ over the zonal direction as

$$\overline{f}(y,t) = \frac{1}{2\pi l_x}\int_0^{2\pi l_x} f(x,y,t)dx. \tag{8}$$

where $f(x,y,t)$ is a generic function. We can therefore set

$$\omega = \Omega + \sqrt{\alpha}\tilde{\omega}, \qquad u = U + \sqrt{\alpha}\tilde{u}, \qquad v = \sqrt{\alpha}\tilde{v}\,, \tag{9}$$

where $\Omega(y,t) = \overline{\omega}(y,t)$, $U(y,t) = \overline{u}(y,t)$ and $\overline{v}(y,t) = 0$ as a consequence of periodicity. The tilde on the variables indicates the perturbation part. We then insert Eq.(9) into Eq.(3), average over x and obtain

$$\partial_t\Omega = -\alpha\overline{v\omega} - \alpha\Omega - \nu(-\partial_y^2)^p\Omega\,. \tag{10}$$

We subtract Eq.(10) from Eq.(3) and drop the tilde to obtain an equation for the non-zonal perturbations

$$\partial_t\omega = -U\partial_x\omega - v\partial_y\Omega - \sqrt{\alpha}\nabla\cdot(\boldsymbol{v}\omega) - \alpha\omega - \beta v - \nu(-\Delta)^p\omega\,. \tag{11}$$

To obtain the quasi-linear approximation, we neglect the non-linear part in Eq.(11) (eddy-eddy interactions) and set $\Omega(y) = -\partial_y U(y)$ where we get the quasi-linear (QL) system

$$\begin{cases} \partial_t U = \alpha\overline{v\omega} - \alpha U - \nu(-\partial_y^2)^p U \\ \partial_t\omega = -U\partial_x\omega - (\partial_y^2 U - \beta)v - \alpha\omega - \nu(-\Delta)^p\omega + \sqrt{2}\eta\,. \end{cases} \tag{12}$$

The non-linear term should be negligible at leading order with the rescaling we have applied. The $\overline{v\omega}$ term in the mean velocity evolution equation in Eq.(12) represents the perturbation Reynolds stress divergence and acts as the influence of the perturbations on the mean flow. In the absence of dissipation and forcing, the QL system conserves energy

$$E_{QL} = \frac{1}{2}\int_{\mathcal{D}}(\overline{\boldsymbol{v}}^2 + \tilde{\boldsymbol{v}}^2)d\boldsymbol{r}, \tag{13}$$

and as the averaging is carried out over x, the invariants (energy, potential enstrophy) of the QL system are equal to that of the non-linear system (Eq.(3)). QL dynamics are an approximation of the NL dynamics, however, the main motivation for adopting the QL approximation is that it produces the expected qualitative behaviour of jet emergence and stability. Srinivasan et al.[6] compared the QL system to the NL system and showed that the QL jets are generally faster than the NL counterparts and so the QL system is more zonostrophically unstable. However,

important flow features such as the invariants and symmetries are conserved and so the QL system is useful for identifying the mechanisms necessary for jet emergence. Bouchet et al.[19] proved that the solutions of the QL system correspond quantitatively to the NL system only in the case of $\alpha \ll 1$ which is the case that we are considering in this report.

It can clearly be seen that time-scale separation exists between the fast fluctuations which are of order one and the slow mean velocity evolution which is of order $1/\alpha$. If we consider the evolution of ω whilst keeping U fixed, the perturbation evolution equation will be linear. The distribution of ω is then completely represented by the perturbation two-point correlation function $g(\boldsymbol{r}_1, \boldsymbol{r}_2, t) = \mathbb{E}[\omega(\boldsymbol{r}_1, t)\omega(\boldsymbol{r}_2, t)]$ where the expectation is taken over the realisations of the noise. Evolving g as opposed to the perturbation equation in Eq.(12) is the S3T method first proposed by Farrell and Ioannou[21]. S3T is, therefore, an approximation of the QL system dynamics as the perturbation Reynolds stress divergence is replaced with its ensemble average while keeping U fixed.

B. Energy Balance

We now carry out an energy balance for the QL system. We can define the Reynolds stress as

$$R_U(y) = \int_{\mathcal{D}} \left(\partial_x \Delta_y^{-1} C(x, y, x', y')\right)_{(x,y)=(x',y')} \, dx \,, \tag{14}$$

where $C(x, y, x', y') := \omega(x, y)\omega(x', y')$. Let E_U be the zonal energy,

$$E_U = \pi \int_{\mathcal{D}} \mathbb{E}[U^2] \, dy \,. \tag{15}$$

Plugging this into the first equation in Eq.(12) and setting the time derivative to zero for stationarity gives

$$E_U = \pi \int_{\mathcal{D}} \mathbb{E}[U R_U] \, dy - \frac{\pi\nu}{\alpha} \int_{\mathcal{D}} \mathbb{E}[(\partial_y U)^2] \, dy \,. \tag{16}$$

The first term describes the energy production due to the non-zonal fluctuations and the last term is the expected energy dissipation. Carrying out the same steps for the non-zonal energy gives

$$E_\omega = -\frac{\nu}{2} \int_{\mathcal{D}} \mathbb{E}[C_{(x,y)=(x',y')}] \, dx \, dy - \frac{1}{2} \int_{\mathcal{D}} \mathbb{E}[U R_U] \, dx \, dy + 1, \tag{17}$$

where the forcing is normalised such that the energy input is unity and the first term is the fluctuation energy dissipation. We can therefore obtain the total stationary energy , $E = E_U + E_w$,

$$E = 1 - \frac{\nu}{2} \left(\int_{\mathcal{D}} \mathbb{E}[C_{(x,y)=(x',y')}] \, dx \, dy + \frac{2\pi}{\alpha} \int_{\mathcal{D}} \mathbb{E}[(\partial_y U)^2] \, dy \right). \tag{18}$$

The time-scale separation of α between the zonal flow and non-zonal fluctuations can be seen in the stationary energy as when $\alpha \ll 1$, the energy in the non-zonal fluctuations is of order one. We can see from this energy balance that there does exist an inverse energy cascade as energy is being transferred from the small-scales to the large-scales. In the turbulent inertial regime of $\nu \ll \alpha \ll 1$, the stationary energy will be $E \approx 1$.

C. Numerical Computation

We integrate the QL system Eq.(12) using spectral methods on a 128×64 ($N_y \times N_x$) grid with de-aliasing using the 2/3 rule. Consider the Fourier expansion of the vorticity field

$$\omega(x, y, t) = \sum_{k,l} \hat{\omega}_{k,l}(t) e^{ikx + ily}, \tag{19}$$

we can then write the vorticity equation of Eq.(12) explicitly in terms of the Fourier components which takes the form

$$\partial_t \hat{\omega}_{k,l} = -ik\hat{U}_l\hat{\omega}_{k,l} + (l^2\hat{U}_l - \beta)\hat{v}_k - \alpha\hat{\omega}_{k,l} - \nu(k^2+l^2)^p\hat{\omega}_{k,l} + \sqrt{2}\hat{\eta}_{k,l}. \tag{20}$$

We carry out the same procedure for the velocity evolution equation of Eq.(12) and integrate the ordinary differential equations (ODEs) using an exponential time differencing scheme (ETD1)[28]. For a system of ODEs in a spatial domain $D = [0, 2\pi]^d \subset \mathbb{R}^d$ and for a time $t > 0$

$$\partial_t \boldsymbol{u} = \boldsymbol{L}\boldsymbol{u} + \boldsymbol{N}(\boldsymbol{u}, t) \tag{21}$$

where $\boldsymbol{L}$ is a linear operator acting on u and $\boldsymbol{N}$ is a non-linear operator, the ETD1 scheme is given by multiplying the above equation by an integrating factor $e^{\boldsymbol{L}h}$ and integrating to give

$$\boldsymbol{u}_{n+1} = e^{\boldsymbol{L}h}\boldsymbol{u}_n + \boldsymbol{L}^{-1}(e^{\boldsymbol{L}h} - \boldsymbol{I})\boldsymbol{N}(\boldsymbol{u}_n, t_n) \tag{22}$$

where $\boldsymbol{I}$ is the identity matrix, h is the time-step and a first order approximation is used for the non-linear integral term. With this scheme, the computation of the linear terms is very efficient and exact with the non-linear part assumed to be constant between t_n and t_{n+1}. ETD is used to integrate stiff systems and in our system (Eq.(12)) the hyper-viscosity term provides the harshest stability condition which is treated with ETD. When $\boldsymbol{L}$ is small, the scheme approaches the forward Euler method. These schemes have a realistic representation of high frequencies and have better accuracy than semi-implicit schemes[28]. ETD includes matrix exponentials and inversions which can be very costly to compute, however, the terms $e^{\boldsymbol{L}h}$ and L^{-1} can be computed before iterating the system which makes the computational cost negligible.

Of course, this scheme can be expanded to include variable time stepping and Runga-Kutta on the non-linear term such as ETDRK4[28]. However, for our chosen parameters, the ETD1 scheme was sufficient. ETD schemes have been largely used in physics applications such as atmospheric dynamics[6] and magnetohydrodynamics (MHD)[29].

D. Numerical Results

We integrate the QL system Eq.(12) with $\alpha = 0.01$, $\nu = 1 \times 10^{-6}$, $l_x = 1$ and $p = 2$. Such low hyper-viscosity dissipates flow at the smallest scales and can be assumed to be negligible in the global energy balance, however, we retain hyper-viscosity for numerical stability. For the initial conditions, we use $U_0 = \sin(ny)$ and $\omega_0 = 0$ where n is the number of jets. Figure 3 shows a stable configuration of four jets starting from an unstable two jet configuration which is achieved through splitting events of prograde jets when $\beta = 4.5$. This jet structure can also be seen in the velocity profile plots. Interestingly, when $\beta = 1$, no stationary jet configuration has been reached after long times as shown in Figure 3. This is a result of a low planet vorticity gradient which causes more instability in zonal structures (zonal structures have a larger growth rate with small β)[23]. The velocity profile for the unstable ($\beta = 1$) configuration looks very similar (smaller magnitude) to the velocity profile of the stationary configuration, however, this can be deceiving as there are clearly no stable jets. We can therefore see that by having a different β value, the jet configuration can be dramatically affected. These integrations of the QL system took two hours on average which would make investigating the parameter space extremely inefficient and computationally very costly.

We can also numerically compute the energy balance in the system to verify the assumptions on smallness for viscosity and scale separation between the zonal and non-zonal flows. The left plot in Figure 4 shows the energy evolution for $\beta = 4.5$ which converges to the stationary energy predicted by the stationary energy balance Eq.(18). This confirms our viscosity smallness assumption as the stationary energy is close to unity. The right contour plot of the vorticity field in Figure 4 shows that zonal bands develop in regions of jets in the velocity profile, therefore, the small scale structures have become anisotropic and sheared zonally due to the jets. This is the shear-straining mechanism that is thought to cause jet organisation.

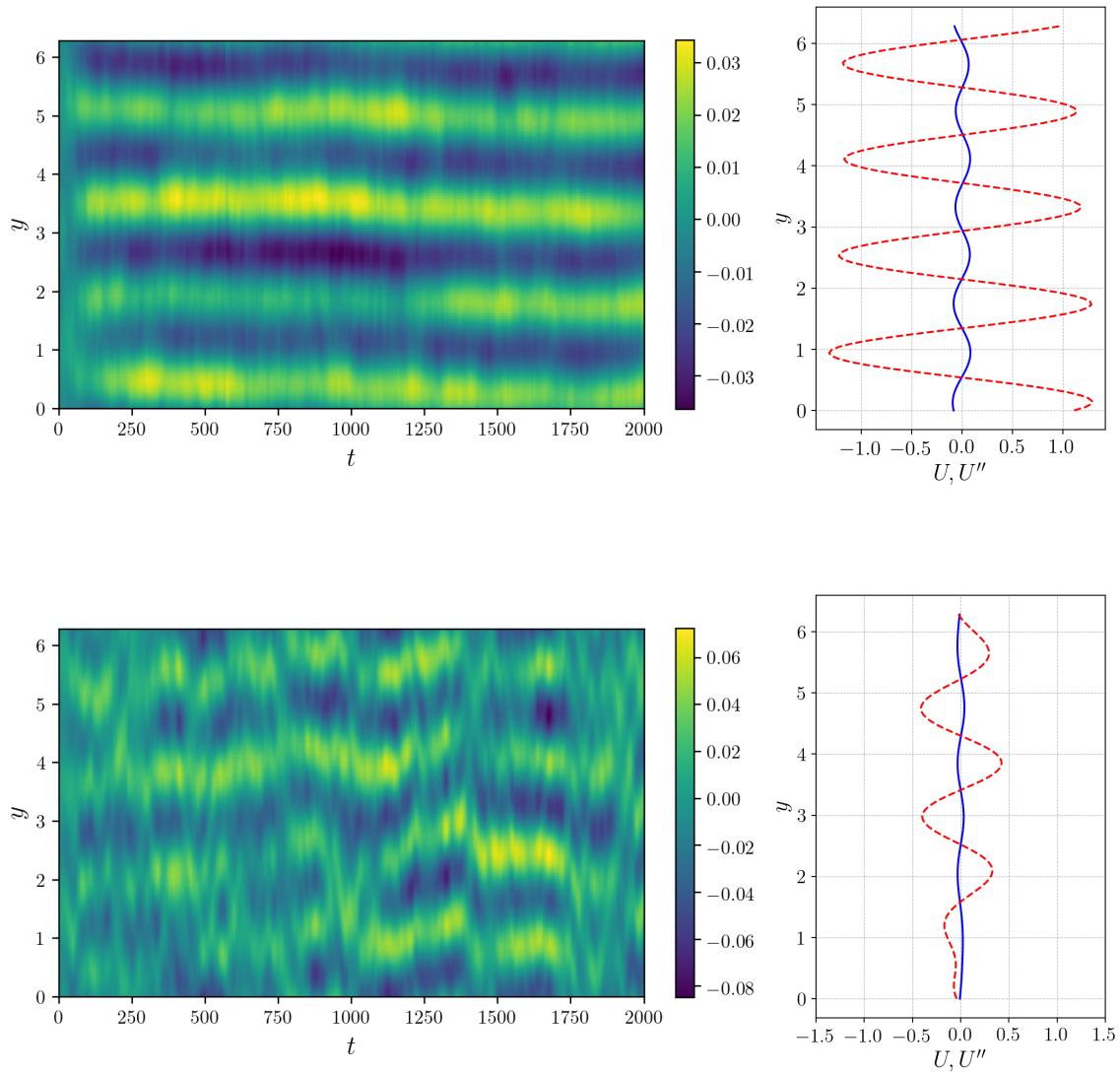

FIG. 3: Top-left: Hovmöller diagram of $U(y,t)$ showing jet emergence and stability of four jets by integration of Eq.(12) with $\alpha = 0.01$, $\beta = 4.5$, $\nu = 1 \times 10^{-6}$, $p = 2$, $h = 0.001$, $U_0 = sin(2y)$, $k_* = 11$ and $\delta k = 1$. Bottom-left: Hovmöller diagram of $U(y,t)$ showing no stable jet configurations when $\beta = 1$. Top-right and bottom-right: Shown is $U(y, t = 2000)$ (solid blue line) and $U''(y, t = 2000)$ (dashed red line) where the stationary (unstable in the case of the bottom plot) velocity jet profile can be seen.

IV. STOCHASTIC AVERAGING AND LARGE TIME-SCALE SEPARATION

For the QL system Eq.(12) and NL system Eq.(3) dynamics, there exist parameter ranges where multiple fixed points (meta-stable jet configurations) exist. We want to compute these fixed points much more efficiently than through analysing the NL and QL systems.

We will now introduce stochastic averaging which is a tool that can be used to study the dynamics of a system with a fast evolving stochastic process coupled to a slowly evolving variable. Consider a fast-slow stochastic dynamical

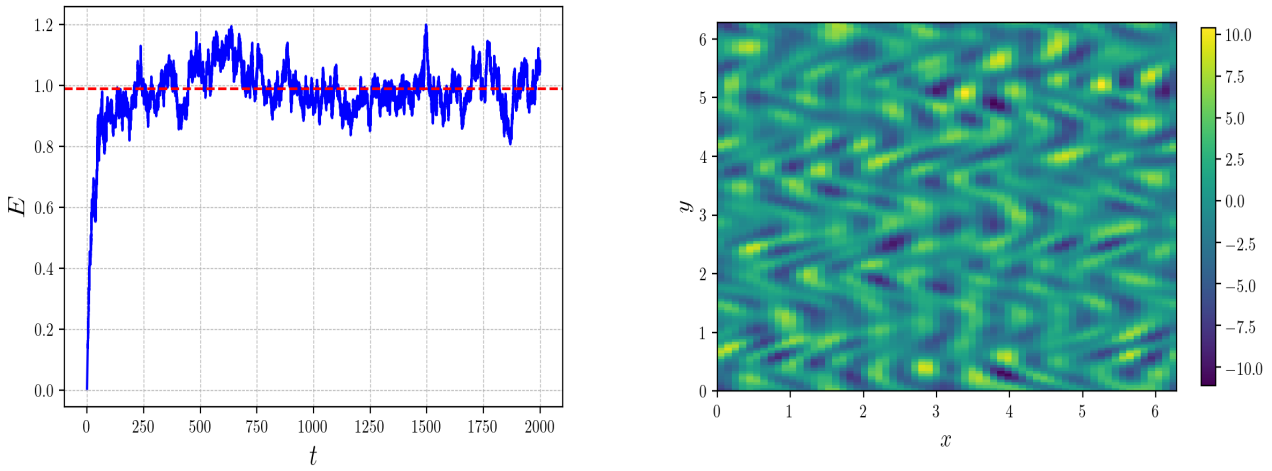

FIG. 4: Left: Total energy evolution in the system (solid blue line) for $\alpha = 0.01$, $\beta = 4.5$, $\nu = 1 \times 10^{-6}$, $p = 2$, $h = 0.001$, $U_0 = \sin(2y)$, $k_* = 11$ and $\delta k = 1$. Theoretical stationary energy (dashed red line) computed from Eq.(18) is also shown. Right: Vorticity contour plot $\omega(x, y, t = 2000)$ showing shearing of small scale structures.

system

$$\begin{cases} \partial_t X = f(X, Y) \\ dY = \frac{1}{\alpha} b(X, Y)dt + \frac{1}{\sqrt{\alpha}} \sigma(X, Y)dW(t), \end{cases} \tag{23}$$

where $f : \mathbb{R}^m \times \mathbb{R}^n \to \mathbb{R}^m$ and $b : \mathbb{R}^m \times \mathbb{R}^n \to \mathbb{R}^n$ are vector fields, $W(t) \in \mathbb{R}^p$ is a standard Wiener process, $\sigma : \mathbb{R}^{m\times n} \to \mathbb{R}^{n\times p}$ and $0 < \alpha \ll 1$ (see ref[30]). In this system, the variable X evolves on a time-scale of order $1/\alpha$ and Y evolves on a time-scale of order one. Therefore, large time-scale separation is present in the system when $\alpha \ll 1$. The aim of stochastic averaging is to give the dynamical behaviour of X on a time-scale order of $1/\alpha$ whilst the contributions of Y on X have been averaged out.

We can represent our QL system in the form of Eq.(23) as

$$\begin{cases} \partial_t U = \overline{v\omega} - U - \nu(-\partial_y^2)^p U \\ d\omega = -\frac{1}{\alpha}\Gamma(U)\omega\, dt + \sqrt{\frac{2}{\alpha}}\sigma dW(t) \end{cases} \tag{24}$$

where the vorticity evolution equation is a stochastic PDE and an Ornstein-Uhlenbeck process with drift

$$\Gamma(U) = U\partial_x + (\partial_y^2 U - \beta)\partial_x \Delta^{-1} + \alpha + \nu(-\Delta)^p\,. \tag{25}$$

To obtain Eq.(24), we have rescaled time by α, replaced the unimportant viscosity ν with $\alpha\nu$ and $\sigma\sigma^\dagger = \chi$ (where $(.)^\dagger$ is the Hermitian transpose). Dissipation of order α is present in the drift term which is different from Eq.(23), therefore, there will be some α dependence in the slow zonal evolution equation. The system Eq.(24) can be discretised to be of form

$$\dot{X}_i = \sum_{j,k} y_j M_{i,j,k} y_k + RX_i$$
$$dy_j = -\sum_k \Gamma_{j,k} y_k\, dt + \sum_k \sigma_{j,k} dW_k$$

where R is a constant and M is a symmetric matrix and is studied by Bouchet et al.[30] as a test case. As we will see next, in the limit $\alpha \to 0$, we can write down a law of large numbers (LLN) for Eq.(24).

A. Virtual-fast process

The dynamics of the velocity field (U) is obtained by stochastic averaging and the dynamics of the vorticity (ω) is approximated by its stationary dynamics while having U fixed. In systems such as Eq.(23), the statistics of Y are very close to a "virtual fast process", $\tilde{Y}_x$, with $X = x$ held fixed due to time-scale separation at leading order. If $1 < \delta t \ll 1/\alpha$, then over a time interval of $[t, t + \delta t]$, the zonal velocity profile $U(t)$ has hardly changed while the turbulent vorticity fluctuations $\omega(t)$ can be assumed to be independent as the vorticity evolves on a time-scale order of one. It is therefore natural to introduce a virtual fast process while keeping the slow variable fixed. The virtual fast process is only valid when a time-scale separation exists between the variables X and Y in Eq.(23). We can define such a process for our system Eq.(24) in the limit $\alpha \to 0$ as

$$d\tilde{\omega}_u = -\Gamma(u)\tilde{\omega}_u d\tau + \sqrt{2}\sigma dW(\tau)\,, \tag{26}$$

where the zonal velocity is held fixed $U = u$ and we rescale time to the natural time-scale of the zonal flow , $\tau = t/\alpha$. Let $g(U, w) := \overline{v\omega} - U - \nu(-\partial_y^2)^p U$, we assume that the virtual fast process is ergodic at every u with respect to the invariant measure $\mu_u(d\omega)$ and so the following expectation exists[30]

$$\begin{aligned} G(U) &= \int g(U, w)\mu_u(d\omega) \\ &= \lim_{T\to\infty} \frac{1}{T}\int_0^T g(u, \tilde{\omega}_u(\tau))\, d\tau, \end{aligned} \tag{27}$$

where in the second line we have used ergodicity of the long-time average being equal to the phase-space average. Then there exists an LLN for the mean $\overline{U}$ (formal derivation given by Bouchet et al.[30])

$$\mathbb{P}(|U(t) - \bar{U}(t)| < \epsilon) \to 1 \quad \forall t, \text{ as } \quad \alpha \to 0 \tag{28}$$

where $\epsilon > 0$. The evolution equation for $\overline{U}(t)$ is then given by

$$\begin{aligned} \partial_t \bar{U} &= \mathbb{E}_{\bar{U}}\left[\overline{\tilde{\omega}_{\bar{U}}\tilde{v}_{\bar{U}}}\right] - \bar{U} - \nu(-\Delta)^p\bar{U} \\ &= \frac{1}{L}\int \left(\partial_x\Delta^{-1}\mathbb{E}_{\bar{U}}\left[\tilde{\omega}_{\bar{U}}(x, y)\tilde{\omega}_{\bar{U}}(x', y')\right]\right)_{y=y', x=x'} dx - \bar{U} - \nu(-\Delta)^p\bar{U}\,, \end{aligned} \tag{29}$$

where $\tilde{v}_u$ is the velocity corresponding to the vorticity of the virtual fast process. The assumption of ergodicity implies that the solution of S3T[6,21] in the limit of large time-scale separation converges to the LLN equation Eq.(29). We can write down the invariant measure of the virtual fast process as it is an Ornstein-Uhlenbeck process which is a linear stochastic process and the correlation matrix of the virtual fast process $C_{\bar{U}}(x, y, x', y') = \mathbb{E}_{\bar{U}}\left[\tilde{\omega}_{\bar{U}}(x, y)\tilde{\omega}_{\bar{U}}(x', y')\right]$ fulfills the stationary Lyapunov equation

$$\Gamma(\bar{U})C_{\bar{U}} + C_{\bar{U}}\Gamma(\bar{U})^\dagger = 2\sigma\sigma^\dagger\,, \tag{30}$$

which we obtain by applying Ito's formula to Eq.(26). That is, the Lyapunov equation Eq.(30) has a unique stationary solution when the virtual fast process Eq.(26) has an invariant measure. This property can be shown numerically by integrating the virtual fast process for long times and comparing the covariance with that of the the Lyapunov equation Eq.(30) solution. This comparison is shown in Figure 5 for one zonal wavenumber ($k = 1$) for simplicity and it holds for all zonal wavenumbers. The virtual fast process was integrated using the Euler–Maruyama[31] method with samples taken at stationarity to compute the covariance. As χ is a function of distances instead of absolute coordinates (Eq.(6)), χ is rebuilt to Toeplitz form (for translational invariance) which if all zonal wavenumbers are to be considered, would be a tensor of size $N_y \times N_x \times N_y \times N_x$ (or $N_yN_x \times N_yN_x$), therefore, only a single wavenumber was considered which reduces dimensionality to $N_y \times N_y$ and significantly reduces computational cost. Figure 5 shows that the structure and magnitude of both covariance functions is very similar with even a small number of samples ($N = 200$) which confirms Eq.(30) for our system.

We can therefore conclude that the zonal dynamics can be modelled by the solution of the LLN Eq.(29) in the limit of infinite time-scale separation $\alpha \to 0$,

$$\partial_t \bar{U} = \frac{1}{L}\int \left(\partial_x\Delta^{-1}C_{\bar{U}}(x, y, x', y')\right)_{y=y', x=x'} dx - \bar{U} - \nu(-\Delta)^p\bar{U}\,, \tag{31}$$

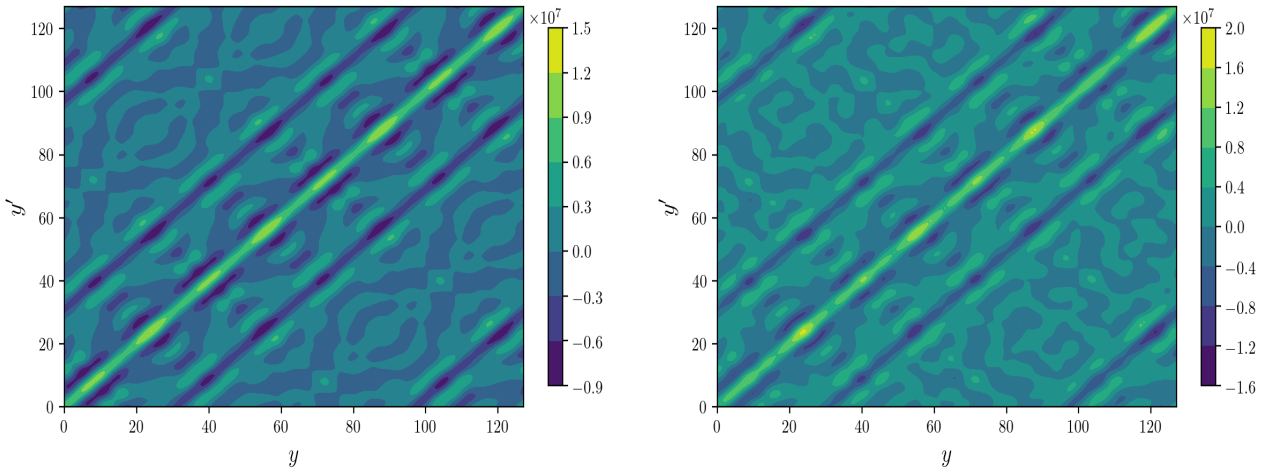

FIG. 5: Left: Contour plot showing $C_{\bar{U}}$ computed from the Lyapunov equation Eq.(30) for a single zonal wavenumber ($k = 1$) Right: Showing numerical covariance $\tilde{\omega}_{\bar{U}}(x, y)\tilde{\omega}_{\bar{U}}(x', y')$ computed from integrating Eq.(26) for a single zonal wavenumber ($k = 1$).

where we can compute $C_{\bar{U}}(x, y, x', y')$ from the solution of Eq.(30) and the system is now deterministic.

B. Numerical Computation

As stated in the previous section, the solution of the full Lyapunov equation would include computations with extremely large matrices. We can therefore use the property of translational invariance in the zonal direction and linearity in $\Gamma(U)$ to simplify the computation greatly. Our computational domain is discretised such that the y-direction is kept in real space with N_y grid points and the x-direction is in Fourier space with N_x grid points. The vorticity can be expanded in zonal harmonics without loss of generality such that

$$\omega(x, y, t) = \sum_k \hat{\omega}_k(y, t) e^{ikx} \,, \tag{32}$$

for the Fourier coefficients $\hat{\omega}_k(y, t)$. Therefore, $\Gamma(U)$ decouples in k and the forcing is chosen such that it separates in k a-priori, so we can compute the Lyapunov equation Eq.(30) independently for each k. We can rewrite the Reynolds stress term in Eq.(31) and so the algorithm in total reads

$$\partial_t U(y) = \sum_{k=0}^{N_x/2} \text{diag}\left[-2k(\partial_y^2 - k^2)^{-1} \Im\left[C_k(y, y')\right]\right] - U(y) - \nu(-\Delta)^p U(y) \tag{33}$$

where for each t and all k the matrix C_k is defined by

$$\Gamma_k(U) C_k + C_k \Gamma_k(U)^\dagger = 2\sigma_k \sigma_k^\dagger \,, \tag{34}$$

in the regime $\nu \ll \alpha \ll 1$ where $C_k, \Gamma_k(U) \in \mathbb{C}^{N_y \times N_y}$, $\sigma_k \in \mathbb{R}^{N_y}$, diag$[A]$ is the main diagonal of matrix A and $\Im[B]$ is the imaginary part of B. The matrix $\Gamma_k(U)$ is of the form

$$\Gamma_k(U) = \mathrm{i}k \underbrace{\begin{pmatrix} U_1 & & \\ & \ddots & \\ & & U_{N_y} \end{pmatrix}}_{\equiv U} + \mathrm{i}k \underbrace{\begin{pmatrix} \mathrm{d}^2U_1/\mathrm{d}y^2 - \beta & & \\ & \ddots & \\ & & \mathrm{d}^2U_{N_y}/\mathrm{d}y^2 - \beta \end{pmatrix}}_{\equiv \mathbb{D}_y^2 U - \beta} \left(\mathbb{D}_y^2 - k^2\mathbb{I}\right)^{-1}$$
$$+ \alpha\mathbb{I} + \nu\big(-\mathbb{D}_y^2 + k^2\mathbb{I}\big)^p$$

where $\mathbb{D}_y^2$ is the discretised ∂_{yy} operator and $\mathbb{I}$ is the identity matrix. We aim to find fixed points, $\partial_t U(y) = 0$ of the LLN system Eq.(33), therefore we can view the system as a pre-conditioned iterative descent algorithm. As the integration is carried out on only the slow time-scale, the fast variable does not impact the numerical stability with the harshest stability condition imposed by the hyper-viscosity term. As before, we treat both linear terms in Eq.(33) using ETD1 and solve the Lyapunov equation using the Bartels-Stewart algorithm[32] implemented by the `solvecontinuouslyapunov` function in Python. We use $N_y = 128$ and $N_x = 64$ for the grid size with the same forcing as when solving the QL system and we obtain the fixed point after only a few iterations.

C. Numerical Results

We integrated Eq.(33) with the same parameters as in the QL system in Section III with $\beta = 4.5$ for comparison. We can see in the left figure of Figure 6 that the solution of the LLN equation found the stable four jet configuration starting from the unstable two jet configuration. The velocity magnitude is very similar between the QL (top-left figure of Figure 3) and LLN systems. The small differences are because time-scale separation is never infinite and the zonal dynamics experience some fluctuations above their mean. However, this still means that the LLN system is a good approximation of QL system dynamics. An interesting observation is that in this LLN system (with these parameters), it is always retrograde jets that split and prograde jets that merge. Computationally, the integration of the LLN system took a maximum of two minutes to find the fixed point; much faster than integration of the QL system. Of course, as α gets smaller, the LLN system solution will approach the QL solution.

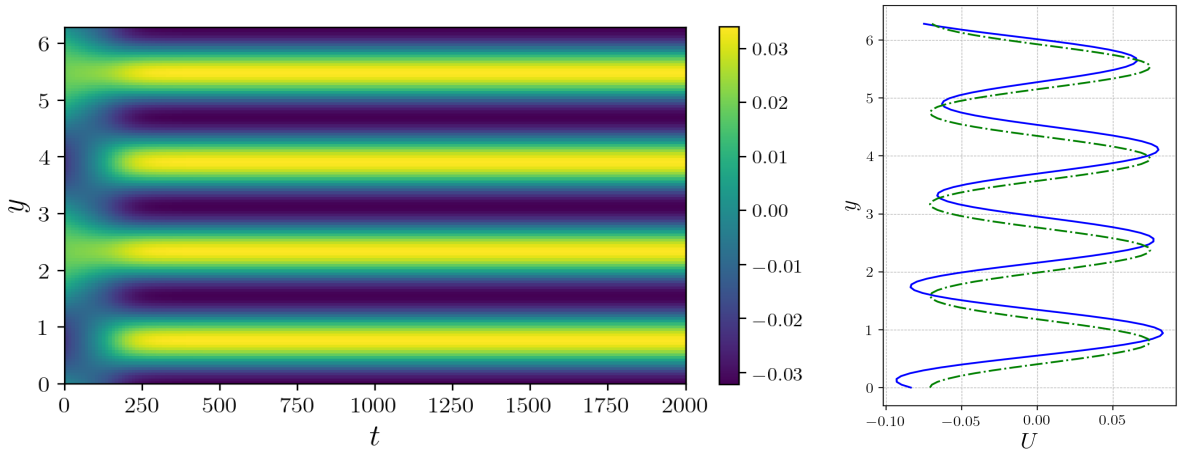

FIG. 6: Left: Hovmöller diagram of $U(y,t)$ showing jet emergence and stability of four jets by integration of Eq.(33) with the same parameters as used in the QL integration with. Right: Velocity profile plot $U(y, t = 2000)$ showing similarity between the QL (solid blue line) and LLN (dash-dotted green line) velocity profiles.

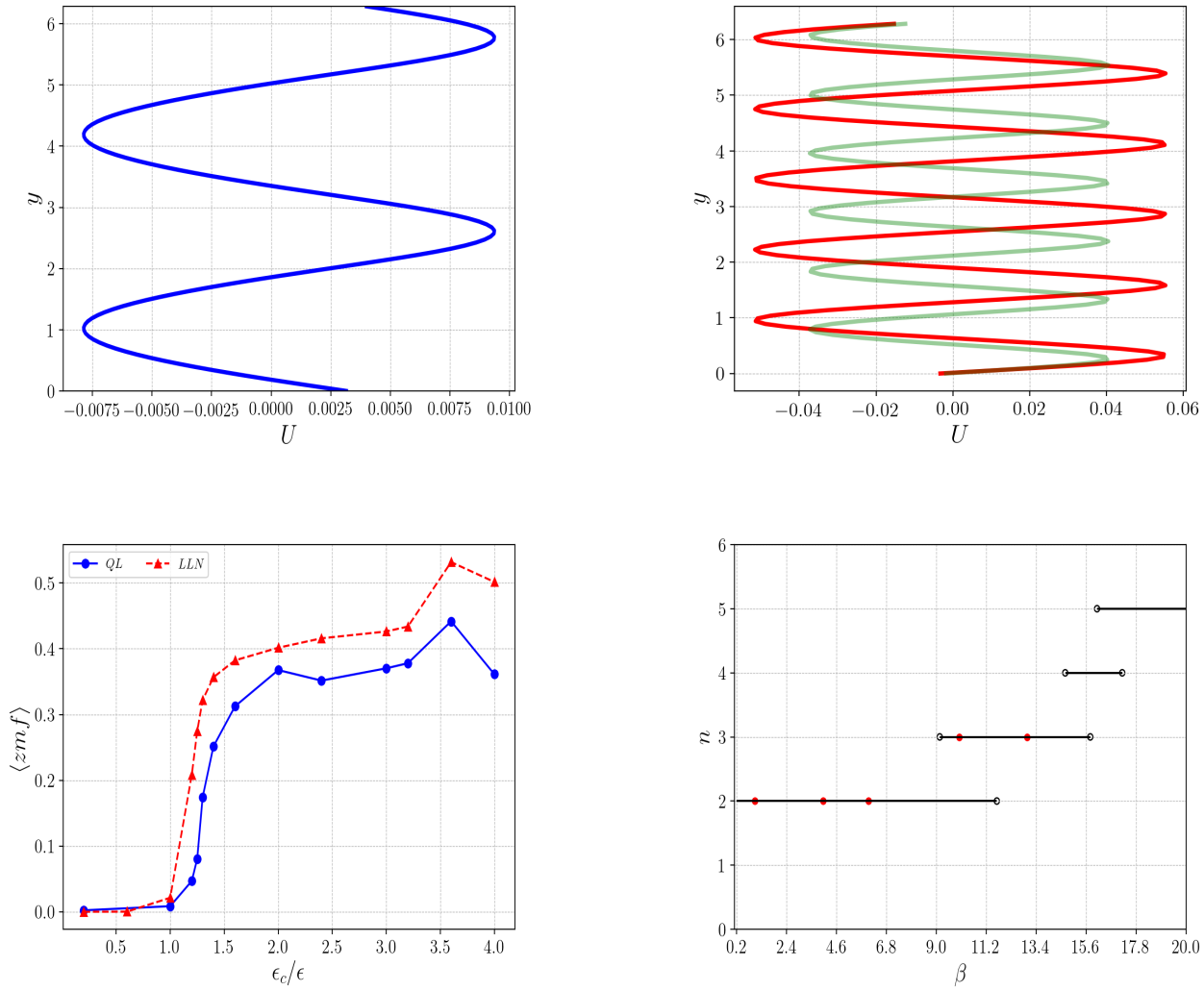

FIG. 7: Top-left: Velocity profile $U(y, t = 2000)$ of the only stable two jet configuration for $\alpha = 2 \times 10^{-4}$ and $\beta = 1.6$. Bottom-left: Comparison of zonal mean flow showing a bifurcation structure with varying energy input rate by unit mass showing between the QL and LLN systems with $\alpha = 0.001$, $\beta = 4.5$, $k_* = 13$ and $\delta k = 1$. Top-right: Velocity profile plot $U(y, t = 2000)$ showing the stable five jet (solid red) and six jet (solid pale green) configurations. Bottom-right: Bifurcation diagram for the number of jets (n) with varying β for $\alpha = 0.0014$, $k_* = 13$ and $\delta k = 1$ where the red points are the QL system solutions.

We can utilise the efficiency of the LLN system to find parameters at which multiple fixed points (jet configurations) are meta-stable. The top figures of Figure 7 show examples of multiple fixed points existing for various parameter values such as when $\alpha = 2\times10^{-4}$ and $\beta = 1.6$, there exists only the one stable jet configuration of two jets. However, when $\alpha = 7 \times 10^{-4}$ and $\beta = 5.3$, both the five and six jet configurations are stable with the five jet configuration having a very small basin of attraction. Therefore, it is very likely that Jupiter did indeed lose a jet as multiple jet configurations can be stable for the same Coriolis parameter according to our numerics.

D. Jet stability in the parameter space

Constantinou et al.[23] states that there exists a critical energy input rate (ϵ_c) which when $\epsilon < \epsilon_c$, no stable coherent zonal structures can exist. Here we show that this property is reproduced by the LLN system dynamics. We define the zonal-mean-flow index[6] as

$$\langle zmf \rangle = E_U/(E_U + E_w), \tag{35}$$

where $\langle . \rangle$ denotes the time average when stationarity is reached. We investigate the zonal-mean-flow index as a function of ϵ. Energy input rate by unit mass is defined as $\epsilon = \gamma/4\pi l_x L^2$ and we vary this parameter by varying γ. The bottom-left figure in Figure 7 shows that this energy input rate bifurcation structure exists in the LLN system as well as the QL system. The critical energy input rate is nearly equal for both systems at $\epsilon_c \approx 500$ which again confirms that the LLN system is a good approximation for QL dynamics. This is an important result as it can help identify which processes lead to jet emergence by analysing the model close to ϵ_c. Stochastic averaging therefore allows much more efficient analysis of such dynamics compared to computations with the QL and S3T systems.

We can vary the planetary rotation parameter β for a given α and study the meta-stable configurations that arise with a planetary rotation bifurcation or stability diagram. The bottom-right figure of Figure 7 shows that as β is increased, the jet configurations with more jets are stable. For the chosen range of $0.1 \leq \beta \leq 20$, the most stable configuration is the two jet configuration and we can see that the QL stationary jet configurations (red points) agree with the LLN results. There are various β values where two meta-stable jet configurations exist such as $\beta = 10$ for two and three jets and $\beta = 16$ for four and five jets. We have only observed saddle points which are transition states between various jet configurations with the parameters that we have tested. This means that the simple LLN system can be used to study the complex stability dynamics of the QL approximation in the inertial limit ($\nu \ll \alpha \ll 1$) which is a very exciting result.

V. CONCLUSION AND FUTURE WORK

In this paper, we have presented a stochastic non-linear system for modelling the emergence and stability of turbulent jets on Jovian atmospheres with the β-effect and barotropic assumptions. We decomposed this system to obtain a quasi-linear approximation of jet dynamics by neglecting the non-linear terms and integrated this system for long times using spectral methods. Zonal jets were observed for certain chosen parameters and an energy balance was numerically verified to confirm our assumptions about time-scale separation. Exploiting the large time-scale separation in the QL system, we applied the classical tool of stochastic averaging to obtain a law of large numbers equation through a heuristic derivation. The stochastic QL system was reduced to a deterministic evolution of mean zonal velocity with averaged non-zonal fluctuations. Integration of the LLN system showed excellent agreement with QL system dynamics with LLN computation being much more efficient compared to the QL system. We have confirmed that the LLN system exhibits the property of a bifurcation at a critical energy input rate ϵ_c where jets will not emerge if $\epsilon < \epsilon_c$ which coincides with that of the QL system. Having been convinced by the LLN results, we varied the Coriolis parameter β where we observed multiple meta-stable fixed points such as the two and three jet configuration being stable at $\beta = 10$.

These results are very promising as it means that the complex QL system can be reduced to a deterministic system using stochastic averaging while retaining most of the dynamics of the original system in the inertial limit. As stated in the introduction of this report, jet emergence and stability are of great interest to the scientific community as jets are present in most planetary atmospheres as well as plasma confinement devices. The tools presented in this report can aid massively in the prediction and stability of jets in both systems which can advance our understanding of atmospheric processes and lead to more efficient plasma confinement.

In the system we have studied in this report, we have assumed complete and clean time-scale separation between the fast and slow variables. In practice, however, the system does not cleanly separate. With our rescaling, the hyper-viscosity term contains an α which in the limit of $\alpha \to 0$ will vanish. Therefore, more work has to be carried out in choosing the correct non-dimensionalisation and as a consequence, the validity of time-scale separation in this system.

Instead of varying the β parameter to study transitions, we can utilise more sophisticated tools such as the string method[33] to compute the heteroclinic orbits connecting various meta-stable states. We can also find unstable fixed points using the minimum action method[34] and the Hamiltonian equations of our system. These methods, however, do not estimate the relative stability of a fixed point, the transition probabilities or the exit times. To more concretely describe the complete dynamics, we can apply both the Central Limit Theorem (CLT) and the Large Deviation Principle (LDP)[30] to our system. The CLT would describe typical fluctuations of the zonal velocity while the LDP would describe the large fluctuations (rare-events). These tools can, of course, be applied to other similar systems with time-scale separation such as the generalised Hasegawa-Mima equation[35] which is a model for magnetised plasma turbulence.

ACKNOWLEDGEMENTS

I would like to thank my supervisor Tobias Grafke for his continuous support throughout this project especially through the tedious technical numerics. I would also like to thank the MathSys team and the EPSRC for funding this project.

REFERENCES

[1]A. P. Ingersoll, "Atmospheric dynamics of the outer planets," Science **248**, 308–315 (1990).
[2]R. Howard, "Torsional oscillations of the sun," in *International Astronomical Union Colloquium*, Vol. 66 (Cambridge University Press, 1983) pp. 437–437.
[3]J. Rogers, *The Giant Planet Jupiter* (Cambridge Univ. Press, Cambridge, 1995).
[4]A. R. Vasavada and A. P. Showman, "Jovian atmospheric dynamics: An update after galileo and cassini," Reports on Progress in Physics **68**, 1935 (2005).
[5]P. B. Rhines, "Waves and turbulence on a beta-plane," Journal of Fluid Mechanics **69**, 417–443 (1975).
[6]K. Srinivasan and W. Young, "Zonostrophic instability," Journal of the atmospheric sciences **69**, 1633–1656 (2012).
[7]P. D. Williams and C. W. Kelsall, "The dynamics of baroclinic zonal jets," Journal of the Atmospheric Sciences **72**, 1137–1151 (2015).
[8]J. Sommeria, S. D. Meyers, and H. L. Swinney, "Laboratory model of a planetary eastward jet," Nature **337**, 58–61 (1989).
[9]G. Di Nitto, S. Espa, and A. Cenedese, "Simulating zonation in geophysical flows by laboratory experiments," Physics of Fluids **25**, 086602 (2013).
[10]T. J. Dunkerton and R. K. Scott, "A barotropic model of the angular momentum–conserving potential vorticity staircase in spherical geometry," Journal of the atmospheric sciences **65**, 1105–1136 (2008).
[11]J. B. Parker and J. A. Krommes, "Zonal flow as pattern formation," Physics of Plasmas **20**, 100703 (2013).
[12]L. Onsager, "Statistical hydrodynamics," Il Nuovo Cimento (1943-1954) **6**, 279–287 (1949).
[13]F. Bouchet and A. Venaille, "Statistical mechanics of two-dimensional and geophysical flows," Physics reports **515**, 227–295 (2012).
[14]R. Robert and J. Sommeria, "Statistical equilibrium states for two-dimensional flows," Journal of Fluid Mechanics **229**, 291–310 (1991).
[15]F. Bouchet and J. Sommeria, "Emergence of intense jets and jupiter's great red spot as maximum-entropy structures," Journal of Fluid Mechanics **464**, 165–207 (2002).
[16]P. Chavanis and J. Sommeria, "Classification of robust isolated vortices in two-dimensional hydrodynamics," Journal of Fluid Mechanics **356**, 259–296 (1998).
[17]B. F. Farrell and P. J. Ioannou, "Statistical state dynamics: a new perspective on turbulence in shear flow," arXiv preprint arXiv:1412.8290 (2014).
[18]U. Frisch, *Turbulence: The Legacy of A. N. Kolmogorov* (Cambridge University Press, 1995).
[19]F. Bouchet, C. Nardini, and T. Tangarife, "Kinetic theory of jet dynamics in the stochastic barotropic and 2d navier-stokes equations," Journal of Statistical Physics **153**, 572–625 (2013).
[20]J. Marston, E. Conover, and T. Schneider, "Statistics of an unstable barotropic jet from a cumulant expansion," Journal of the Atmospheric Sciences **65**, 1955–1966 (2008).
[21]B. F. Farrell and P. J. Ioannou, "Structural stability of turbulent jets," Journal of the atmospheric sciences **60**, 2101–2118 (2003).
[22]N. A. Bakas and P. J. Ioannou, "Emergence of large scale structure in barotropic β-plane turbulence," Physical review letters **110**, 224501 (2013).
[23]N. C. Constantinou, B. F. Farrell, and P. J. Ioannou, "Emergence and equilibration of jets in beta-plane turbulence: applications of stochastic structural stability theory," Journal of the Atmospheric Sciences **71**, 1818–1842 (2014).
[24]E. Weinan, B. Engquist, *et al.*, "The heterognous multiscale methods," Communications in Mathematical Sciences **1**, 87–132 (2003).
[25]J. O. Dada and P. Mendes, "Multi-scale modelling and simulation in systems biology," Integrative Biology **3**, 86–96 (2011).
[26]D. K. Lilly, "Numerical simulation of two-dimensional turbulence," The Physics of Fluids **12**, II–240 (1969).

[27]G. P. Williams, "Planetary circulations: 1. barotropic representation of jovian and terrestrial turbulence," Journal of the Atmospheric Sciences **35**, 1399–1426 (1978).
[28]S. M. Cox and P. C. Matthews, "Exponential time differencing for stiff systems," Journal of Computational Physics **176**, 430–455 (2002).
[29]J. B. Parker, "Zonal flows and turbulence in fluids and plasmas," arXiv preprint arXiv:1503.06457 (2015).
[30]F. Bouchet, T. Grafke, T. Tangarife, and E. Vanden-Eijnden, "Large deviations in fast–slow systems," Journal of Statistical Physics **162**, 793–812 (2016).
[31]P. E. Kloeden and E. Platen, *Numerical solution of stochastic differential equations*, Vol. 23 (Springer Science & Business Media, 2013).
[32]R. H. Bartels and G. W. Stewart, "Solution of the matrix equation ax+ xb= c [f4]," Communications of the ACM **15**, 820–826 (1972).
[33]T. Grafke and E. Vanden-Eijnden, "Numerical computation of rare events via large deviation theory," Chaos: An Interdisciplinary Journal of Nonlinear Science **29**, 063118 (2019).
[34]E. Weinan and E. Vanden-Eijnden, "Minimum action method for the study of rare events," Communications on pure and applied mathematics **57**, 637–656 (2004).
[35]J. B. Parker and J. A. Krommes, "Generation of zonal flows through symmetry breaking of statistical homogeneity," New Journal of Physics **16**, 035006 (2014).